COMPUTATIONALLY EFFICIENT MODELING OF DELAMINATION BEHAVIOR IN LAMINATED COMPOSITES

Khairul Anam[1,2,*], Melanie Todt[1], Heinz E. Pettermann[1]

[1] Institute of Lightweight Design and Structural Biomechanics, TU Wien, Vienna, Austria
[2] On leave from Department of Mechanical Engineering, Brawijaya University, Malang, Indonesia
[*] anam@ilsb.tuwien.ac.at, mt@ilsb.tuwien.ac.at, pettermann@ilsb.tuwien.ac.at

Keywords: Delamination, Laminated Composite, Ply-Level Model.

Summary: *The simulation of progressive delamination in multilayered laminate components under mode I and mode II delamination are presented. Ply-level based modeling strategies are applied for various choices of element types representing the plies including three-dimensional continuum solid, two-dimensional continuum plane strain, shell, and continuum shell elements. The interfaces between the plies are modeled using cohesive zone elements with either finite or zero geometrical thickness. The conventional ply-level modeling strategy based on continuum solid elements is used as reference solution. Double Cantilever Beam and End Notched Flexure set ups are simulated. The delamination behavior of all models is quantitatively compared in terms of nonlinear load-displacement curves and delamination area. The shell-based ply-level model with finite thickness cohesive zone elements provides very good agreement in terms of accuracy of the results and has high computational efficiency. This is very beneficial for simulating delamination in large-scale and complex laminated composite structures.*

1. INTRODUCTION

Laminated composites have been actively investigated in the last few decades. They are widely used in a variety of industries, including aerospace and automotive engineering, due to their exceptional mechanical characteristics such as being lightweight and having excellent specific stiffness, specific strength, and fatigue properties. Despite their superior performance, laminated composites possess complex damage mechanisms such as matrix cracking, fiber breakage, plasticity-like effects, and delamination [1]. Such damage in laminated composites is potentially dangerous because it can significantly reduce the load-carrying capacity, which can lead to failure of the composites structure [2, 3].

Delamination, i.e. inter-laminar fracture, is one of the most dominant defects that arise in laminated composites. Mostly, delamination occurs internally in laminated composites so that damage is barely visible to the naked eye on the composite surface and, consequently, is difficult to detect during service. In engineering applications, delamination is typically initiated by two main factors. Firstly, the delamination can be promoted by geometric and material discontinuities like ply drop-offs, curved and tapered type corners, skin-stiffener interactions, bonded and bolted joints, access holes, and sandwich transitions that occur because of the inevitability of complex structural designs which cause interface tractions in the structure [2, 4]. Secondly, the delamination can also be introduced by tensile and shear loading scenarios that cause interface tractions. Furthermore, delamination in laminated composites will propagate when loads of sufficient magnitude are applied to the structure. In this regard, avoiding delamination, i.e. delamination initiation as well as propagation is the best option for maintaining the load-carrying capacity of laminated composites.

The delamination behavior of laminated composites has been extensively investigated both experimentally and computationally. Experimental methods are utilized to measure the delamination resistance of laminates, namely inter-laminar fracture toughness or critical strain energy release rate. Double Cantilever Beam (DCB) and End Notch Flexure (ENF) test set-ups are the most common experimental tests to examine the delamination behavior under opening mode and shear mode loading conditions, respectively. However, experimental methods are time-consuming, costly, and rarely used to test full scale structures. There, computational methods within the framework of the Finite Element Method (FEM) offer an efficient way for studying the delamination behavior of laminated composites. Moreover, computational methods are capable to predict the nonlinear mechanical behavior under various loading conditions at various length scales [5].

The most common approach that has been used to predict delamination is the Cohesive Zone Model (CZM) [1, 2, 3] which was first introduced in the studies of Dugdale [6] and Barenblatt [7]. In terms of computational effort, the CZM approach is more practical compared to other fracture mechanics based approaches like e.g. the Virtual Crack Closure Technique because of its capability to make predictions without pre-existing cracks [4]. Due to its flexibility, the CZM approach has been used for investigating a variety of fracture problems including delamination behavior and has been proven to be efficient [1].

Typically, laminated composites are geometrically modeled as a stack of homogeneous or-thotropic layers. At meso-scale level, the stack model can be categorized into stacked shell models and stacked continuum models both of which are so called ply-level models where every ply and every interface of the laminate is modeled explicitly. Ply-level models have been widely used by employing various element types for the plies in combination with different cohesive zone modeling techniques. Schwab and Pettermann [8] combined shell elements with finite thickness cohesive zone elements (CZE) to simulate the failure mechanisms due to impact events on fabric reinforced laminated composites. The shared node coupling technique is used to connect the cohesive layer and the adjacent plies. The modeling approaches based on shell elements show accurate results and present an excellent performance in terms of computational efficiency compared to models based on continuum elements. Shell elements can also be connected to zero thickness CZEs by applying tie constraints, more details can be found in the work of Gager and Pettermann [9]. The tie constraint formulation allows for surface based coupling and takes into account the thickness and kinematics of the involved shell elements [9]. Even though this technique offers more flexibility regarding the mesh size of the CZEs and adjacent plies, it is computationally more expensive than shared nodes between both plies [10]. Continuum shell elements can be an option to represent the plies. The cohesive zone is then modeled with zero thickness and coupled to adjacent plies by using tie constraints. Consequently, the degrees of freedom (DOFs) of the CZE nodes will be eliminated [11]. Bae et al. [4] have used plane strain continuum elements in combination with zero thickness CZEs and tri-axial continuum solid elements with zero thickness cohesive elements to examine the delamination behavior of the composites. In terms of elastic response, critical loads, and load–displacement curves, the numerically predicted results based on continuum elements have matched accurately with those obtained by the experiments.

The focus of this paper is on the comparison between different ply-level models in terms of the validity of delamination prediction in laminated composites and computational efficiency. Five different ply-level models including two-dimensional continuum plane strain, shell, continuum shell, and three-dimensional continuum solid elements with zero-thickness CZEs, and shell elements with finite-thickness CZEs are used. DCB and ENF test set ups according to DIN EN 6033 and 6034 standards are investigated, respectively, by using the commercial FEM package Abaqus/Standard 2020 (*Dassault Systèmes Simulia Corp., Providence, RI, USA*). The delamination response of the ply-level models is quantitatively compared including nonlinear load-displacement curves and delamination area. Finally, the computational efficiency is evaluated in terms of the computation time.

2. PLY-LEVEL MODELS

Ply-level modeling approaches with various choices of element types are studied. The modeling strategies of one interface and the adjacent plies are illustrated in Figure 1. Figure 1(a) presents a ply-level model that is composed of shell elements for the plies, together with finite geometrical thickness of CZEs, denoted as SPLF. The constitutive thickness of CZE is set to be equal to the geometrical thickness. The nodes at the midplanes of the shell elements are
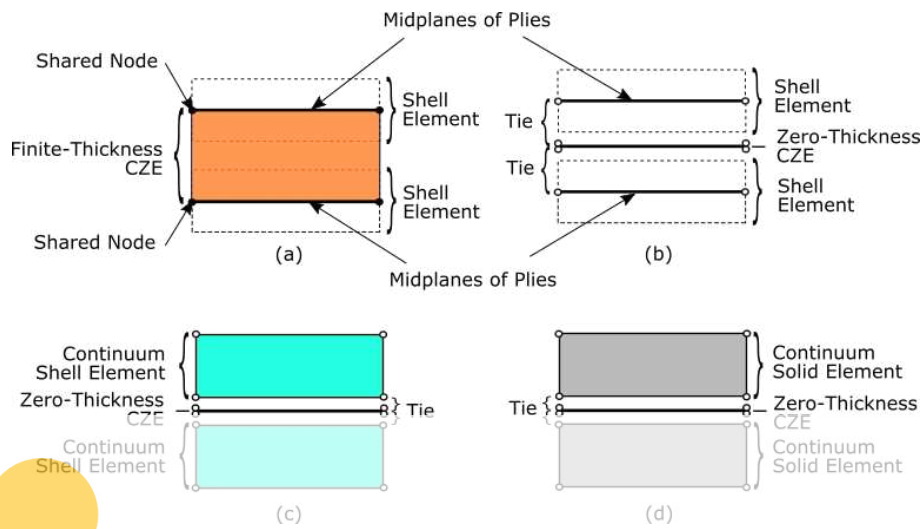
3

Figure 1. Sketch of the coupling technique between one interface and the adjacent plies; (a) finite thickness of CZE with shell elements and zero thickness of CZE with (b) shell elements, (c) continuum shell elements, and (d) continuum solid and continuum plane strain elements.

shared with the nodes of the CZE. In this modeling strategy, the CZE thickness is equal to the adjacent ply thicknesses, i.e. half of the top and bottom ply thickness. Figure 1(b) shows the ply-level model based on shell elements connected to zero geometrical thickness CZE by using surface-to-surface based tie constraints, denoted as SPLZ.

Figure 1(c) presents the ply-level model based on continuum shell elements while Figure 1(d) shows the ply-level model based on two-dimensional continuum plane strain elements and three-dimensional continuum solid elements both of which are coupled to zero geometrical thickness of the CZE. These ply-level models denoted as CSPLZ, CPEZ, and CPLZ, respectively, where the CPLZ model is used as reference model. In CSPLZ, CPEZ, and CPLZ modeling strategy, the surface-to-surface based tie constraints are used as in SPLZ model. The ply surfaces are directly defined from top and bottom surfaces. Generally, for the tie constraint, the surface-to-surface formulation is used to avoid stress noise at tied interfaces [11].

3. APPLICATION EXAMPLES

DCB and ENF simulations are performed to investigate the opening mode (mode I) and shear mode (mode II) delamination, respectively. The modeled laminates comprise eight plies where the CZEs connect all adjacent plies. Five different ply-level models as mentioned in Section 2 are realized.

The overall dimensions, boundary conditions, and loading scenario of the DCB and ENF simulations are illustrated in Figures 2 and 3, respectively. The nominal ply thickness of 0.31625 mm is used leading to the total thickness, $2h = 2.53$ mm. In z-plane view, each ply is discretized using a regular mesh with an element size of $l_x = 0.158125$ mm and $l_y = 1.0$ mm. The mesh around the initial delamination is visualized in Figure 4. To ensure the stability of the
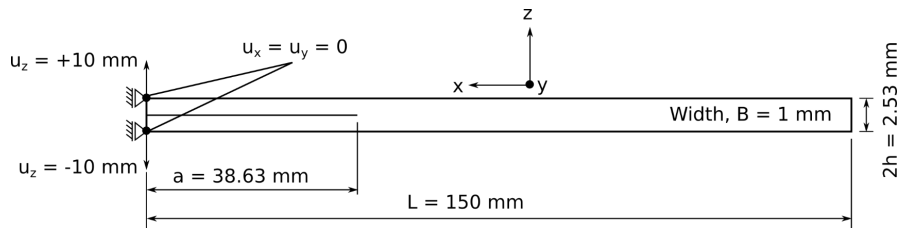
Figure 2. The overall dimensions, boundary conditions, and loading scenario used in the DCB simulations
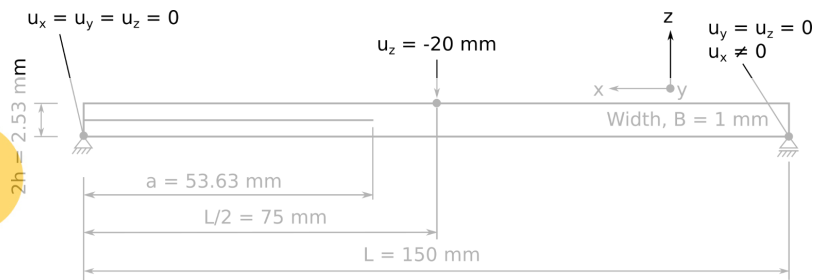

Figure 3. The overall dimensions, boundary conditions, and loading scenario used in the ENF simulations

delamination propagation, the initial delamination length, a, in the ENF model is longer than in the DCB model [12]. Plane strain condition in y-direction is imposed to mimic the large scale model of laminated composite where strains ε_{yy}, γ_{xy}, and γ_{yz} are set to be zero. Moreover, to avoid convergence issues, viscous regularization with a relaxation time of 10^{-4} s is applied in the constitutive law of the CZEs.

A woven carbon fiber reinforced composite is used as the material of the plies which are modeled as linear elastic where the material properties are taken from [13, 14], see Table 1.

The constitutive response of the CZEs is defined using the Abaqus built-in traction-separation law. Damage initiation of the CZEs is predicted according to a quadratic nominal stress criterion [11]. Damage evolution is modeled based on the critical energy release rate in combination with a linear softening relation. For completeness, the mixed-mode conditions are prescribed with the Benzeggagh and Kenane criterion [15], where the parameter upon damage initiation η of 2.0 is chosen. Table 2 lists the CZE properties describing the constitutive response of the

Table 1. Homogenized ply material properties of a woven carbon fiber reinforced composites.

	from [13]	from [14]
Young's moduli (N/mm^2)	$E_x = E_y = 56589.32$	$^*E_z = 10066.00$
Shear moduli (N/mm^2)	$G_{xy} = G_{xz} = G_{yz} = 4185.86$	
Poisson's ratio	$\nu_{xy} = 0.045$	$^*\nu_{xz} = \nu_{yz} = 0.33$

* only apply to CPEZ and CPLZ

5

Figure 4. The mesh visualization of the plies and CZEs around the initial delamination for different ply-level models.

Table 2. The interface properties defining the initial stiffness together with damage initiation and propagation parameters [16].

	Mode I	Mode II
Initial stiffness, K (N/mm^3)	10^5	10^5
Inter-laminar strength, t (N/mm^2)	60	79.289
Critical energy release rate, G_{c} (N/mm)	0.9	2.0

interface. All CZEs have been assigned the same value of K independent to the geometrical thickness. The inter-laminar strengths, t, are taken from [5]. The critical energy release rates, G_{c}, are taken from values published in [16].

The geometric nonlinear analysis option is utilized since large deformation are taken into

account. A displacement rate of 0.005 mm/s is used. Frictionless contact condition is established for the ENF simulation to prevent penetration of the plies at the initial delamination. The contact interactions within the simulation are prescribed using the surface-to-surface algorithm of Abaqus/Standard. Hard contact with a linear penalty stiffness definition is used. The contact stiffness of SPLF, SPLZ, CSPLZ, and CPLZ is reduced by 42.5 % from the default value of 1 while the contact stiffness of CPEZ is increased by 15 %. Adaptive automatic stabilization is activated to improve convergence. For the dissipated energy fraction, the defaultf value of 2.0×10^{-4} is used and for the automatic damping algorithm, the accuracy tolerance of 0.05 is utilized [11].

4. RESULTS AND DISCUSSION

The following results are soleyly obtained by the means of numerical simulations. The load-displacement curve as well as the delamination area at the maximum load and at the maximum displacement are evaluated. The delamination area is calculated by summing up the area of all fully damaged CZEs which possess a stiffness degradation value of 0.999. Finally, the computational efficiency of the individual models in terms of computation time is evaluated. All simulations are carried out using a standard PC work station with eight CPUs at 2.35 – 3.35 GHz.

4.1 DCB Simulations

The load-displacement predictions of the DCB simulations are presented in Figure 5. Overall, the load-displacement results of all models are in a very good agreement with the reference solution of the CPLZ model. For the SPLF model, the predicted stiffness is larger than for the other models and also the maximum load is slightly higher as can be seen in the enlarged view in Figure 5. The higher stiffnes is a consequence of the finite thickness of the CZEs in the SPLF model in combination with the high stiffness assigned to the CZEs. To address this issue, a modification of the traction-separation based constitutive law can be applied, see e.g. [1].

The process zones (PZ) and the delamination area of the three-dimensional ply-level models are presented in Figure 6. Figure 6(a) shows the PZ at the maximum load, just before the delamination starts to propagate. Proper resolution of the PZ near the delamination tip is important to ensure the accuracy of the simulation of delamination propagation. It has been shown by Falk et al. [17] that 4 - 10 elements are sufficient to reliably predict the delamination growth. For the proposed ply-level models, the number of elements in PZ is between seven and nine elements. Figure 6(b) illustrates the PZ and the delamination area (grey elements) at the end of the loading event.

The delamination areas of all models at the maximum displacement of 20 mm show comparable results and are summarized in Table 3. The delamination area of the SPLF model is slightly larger compared to the other ply-level models. As shown in Figure 5, the structural stiffness of the SPLF model is slightly higher before the maximum load but the delamination starts to propagate at a smaller applied displacement. This causes the differences in delamina-
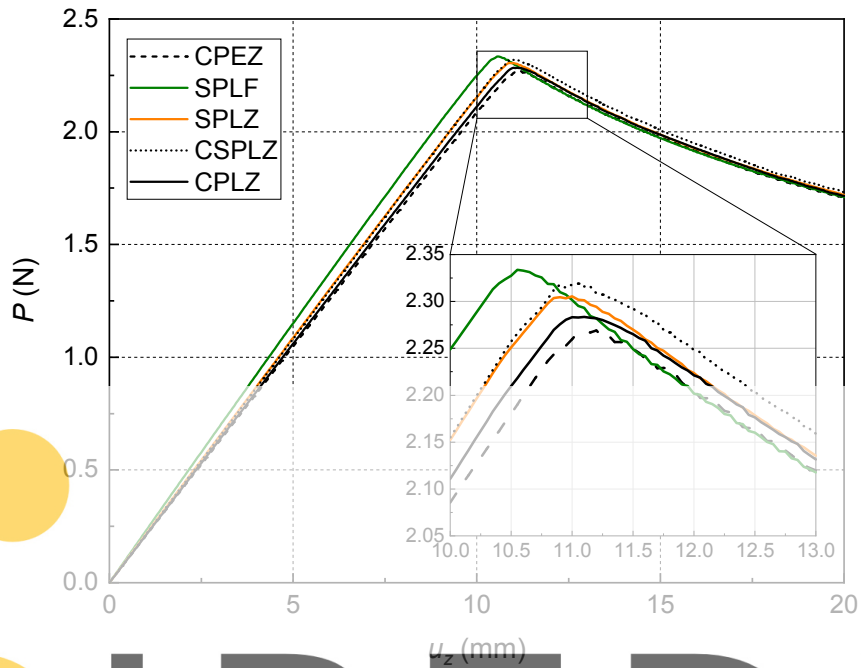
Figure 5. Load-displacement curve of the DCB simulations for different ply-level models.
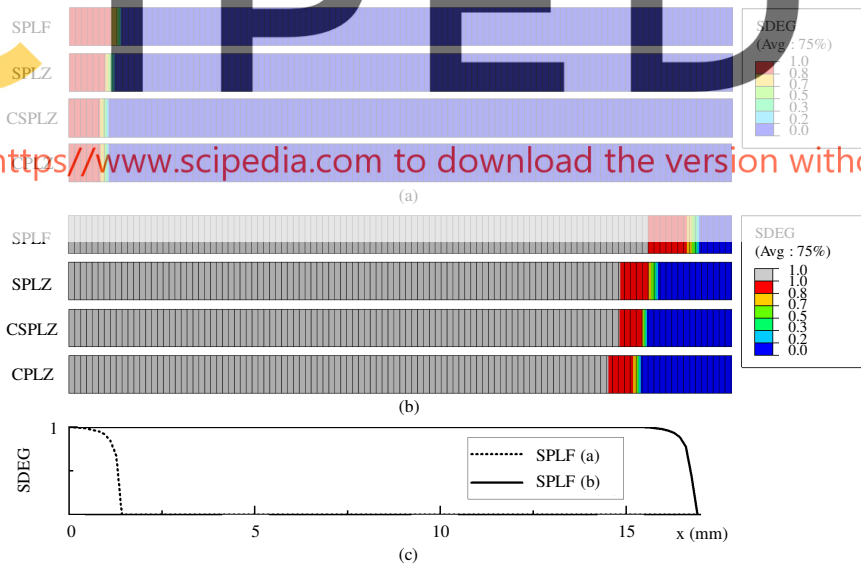

Figure 6. Fracture process zone and delamination area (a) at the maximum load and (b) at the maximum displacement of the DCB simulations. Grey elements represent the fully damaged CZE. (c) shows the stiffness degradation of the SPLF model along x-direction at (a) and at (b).

tion area.

The SPLF model shows a very good computational efficiency compared to the other three-

Table 3. The delamination area, total number of DOFs and computation time of DCB simulations for the ply-level models.

Ply-level models	Delamination Area (mm^2)	Number of DOFs	Computation Time (s)
CPEZ	14.21	30368	425
SPLF	15.47	91104	636
SPLZ	14.68	91104	739
CSPLZ	14.68	91104	1172
CPLZ	14.37	91104	1015

dimensional models, see Table 3. The computation time of the SPLZ model is slightly larger than those of the SPLF model although it uses the same conventional shell elements. This difference is a consequence of the different coupling techniques between plies and CZE as explained in Section 2. The model using three-dimensional continuum and continuum shell elements show a much larger computational time although it has the same number of DOFs as the shell element based ply-level models. This phenomenon indicates that the equation system of the SPLF model solve more efficient compare to continuum based ply-level models. Furthermore, these results indicate that the use of SPLF model can be very beneficial in terms of efficiency when applied to large-scale laminated composite components.

4.2 ENF Simulations

Figure 7 shows the load-displacement curves of the ENF simulations for different ply-level models. The delamination behavior is evaluated by the same approach as for the DCB simulations. The load-displacement curves of the CPEZ, SPLF, and SPLZ models are in very good agreement with those of the CPLZ reference model. Only the CSPLZ shows a different delamination response. There is a delay before the delamination starts to propagate even though the maximum load is close to those of the other models. The reason for this behavior is unclear and will not be discussed any further in this paper. In general, the PZ in the ENF simulations is larger than in the DCB simulations due to the higher critical energy release rate associated with mode II delamination. For the current models, the PZ in the ENF simulations is approximately three times larger than for the DCB test.

The delamination area at the maximum displacement of 20 mm is listed in Table 4 along with the number of DOFs and the computation time. The delamination area of the CPEZ, SPLF, and SPLZ models is the same as for the reference model. Again, the SPLF model provides a very good compromise between computational efficiency with a computation time of around ten minutes and reliable results. The computational time of the SPLF model is even close to those of the CPEZ model which has significantly lower number of DOFs. This difference occurs due to the numerical issues of the model which leads to significantly smaller displacement increments.
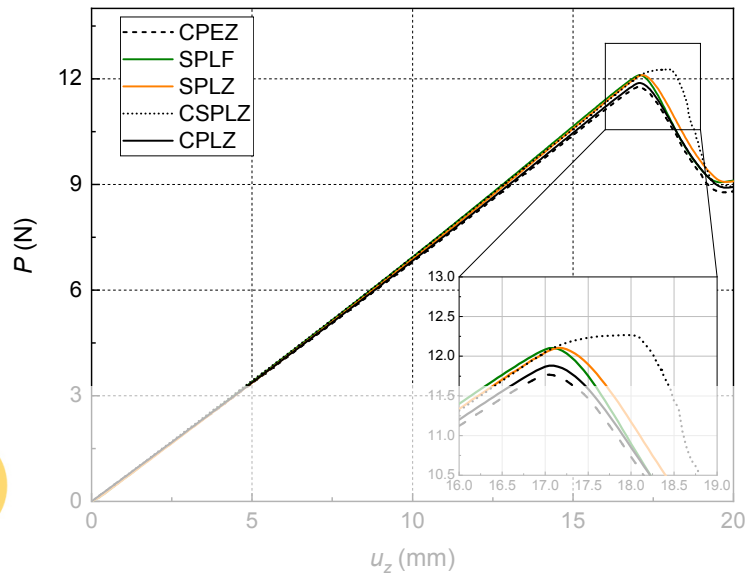
Figure 7. Load-displacement curve of the ENF simulations for different ply-level models.

Table 4. The delamination area, total number of DOFs and computation time of ENF simulations for different ply-level models.

Ply-level models	Delamination Area (mm^2)	Number of DOFs	Computation Time (s)
CPEZ	20.10	30368	509
SPLF	20.10	91104	599
SPLZ	20.10	91104	943
CSPLZ	20.74	91104	1658
CPLZ	20.10	91104	988

5. CONCLUSIONS

A numerical method for studying progressive delamination in laminated composites based on cohesive zone elements is presented. Five different ply-level models are evaluated and compared in terms of load-displacement curves and delamination area. Double cantilever beam and end notch flexure test set-ups are utilized to investigate mode I and mode II delamination. All models show reliable results when compared to continuum element based ply-level models used as reference. The shell based ply-level model with finite thickness cohesive zone elements shows a very good performance in terms of computational efficiency and accuracy of the results. Consequently, the use of this strategy can be very beneficial for simulating delamination in large-scale and complex laminated composite structures.

Acknowledgements

References

[1] M. Schwab, M. Todt, M. Wolfahrt, and H.E. Pettermann, Failure mechanism based modeling of impact on fabric reinforced composite laminates based on shell elements. *Composite Science and Technology*, **128**, 131-137, 2016.

[2] P.P. Camanho, C.G. Davila, and M.F. De Moura, Numerical simulation of mixed-mode progressive delamination in composite materials. *Journal of Composite Materials*, **37**, 1415-1438, 2003.

[3] A. Turon, P.P. Camanho, J. Costa, and J. Renart, Accurate simulation of delamination growth under mixed-mode loading using cohesive elements: Definition of interlaminar strengths and elastic stiffness. *Composite Structures*, **92**, 1857-1864, 2010.

[4] H.S. Bae, M.S. Kang, K.S. Woo, I.G. Kim, and K.H. In, Test and analysis of modes I, II, and mixed-mode I/II delamination for carbon/epoxy composite laminates. *International Journal of Aeronautical and Space Sciences*, **20**, 636-652, 2019.

[5] T. Ceglar, M. Schwab, and H.E. Pettermann, DCB and ENF multi-scale simulations. in: "6th *ECCOMAS Thematic Conference on the Mechanical Response of Composites: COMPOSITES 2017", JJC Remmers, A. Turon (ed.); TU Eindhoven*, (2017), 13-23.

[6] D.S. Dugdale, Yielding of stell sheets containing slits. *Journal of the Mechanics and Physics of Solids*, **8**, 100-104, 1960.

[7] G.I.Barenblatt, The mathematical theory of equilibrium cracks in brittle fracture. *Advances in Applied Mechanics*, **7**, 55-129, 1962.

[8] M. Schwab and H.E. Pettermann, Modeling and simulation of damage and failure in large composite components subjected to impact loads. *Composite Structures*, **158**, 208-216, 2016.

[9] J. Gager and H.E. Pettermann, Numerical homogenization of textile composites based on shell element discretization. *Composite Science and Technology*, **72**, 806-812, 2012.

[10] R. Bogenfeld, J. Kreikemeier, and T. Wille, Review and benchmark study on the analysis of low-velocity impact on composite laminates. *Engineering Failure Analysis*, **86**, 72-99, 2018.

[11] Dassault Systemes Simulia Corp., Providence, RI, USA, Abaqus Analysis User's Guide, Release 2020, 2020.

[12] L. Carlsson, J. Gillespie, and R. Pipies, On the analysis and design of the end notched flexure (ENF) specimen for mode II testing. *Journal of Composite Materials*, **20**, 594-604, 1986.

[13] J. Gager and H.E. Pettermann, FEM modeling of multilayered textile composites based on shell elements. *Composites Part B: Engineering*, **77**, 46-51, 2015.

[14] M. Springer, Nichtlineare Finite Elemente simulation der Schädigungsmechanismen sowie der Resttragfähigkeit von Schlagbeanspruchten Kohlenstofffaser-Epoxidharz-Verbunden. *Master Thesis, TU Wien, Vienna, Austria*, 2014.

[15] M.L. Benzeggagh and M. Kenane, Measurement of mixed-mode delamination fracture toughness of unidirectional glass/epoxy composites with mixed-mode bending apparatus. *Composite Science and Technology*, **56**, 439-449, 1968.

[16] H. Hadavinia and H. Ghasemnejad, Effects of mode-I and mode-II interlaminar fracture toughness on the energy absorption of CFRP twill/weave composite box sections. *Composite Structures*, **89**, 303-314, 2009.

[17] M.L. Falk, A. Needleman, and J.R. Rice, A critical evaluation of cohesive zone models of dynamic fracture. *Journal de Physique IV, Proceedings*, **11**, 543-550, 2001.